energies

MDPI

Article

Inverter Operation Mode of a PhotoVoltaic Cascaded H-Bridge Battery Charger

Marino Coppola *, Pierluigi Guerriero, Adolfo Dannier, Santolo Daliento and Andrea Del Pizzo

Department of Electrical Engineering and Information Technologies, University of Napoli Federico II, Via Claudio 21, 80125 Napoli, Italy; pierluigi.guerriero@unina.it (P.G.); adannier@unina.it (A.D.); daliento@unina.it (S.D.); delpizzo@unina.it (A.D.P.)

* Correspondence: marino.coppola@unina.it; Tel.: +39-081-7683228

Abstract: The paper deals with a grid-connected single-phase battery charger integrated with photovoltaic generators (PVGs). The circuit topology consists of a multilevel architecture based on a Cascaded H-Bridge (CHB) rectifier. Its main task is to charge the batteries, primarily from the PVGs, by also assuring to keep their state-of-charge (SOC) balanced. Nevertheless, when the battery SOC overcomes a predefined upper limit, beyond which the charging process could be interrupted, the available PV power can no longer be transferred to the batteries. Therefore, to avoid an undesired curtailment of PV power production, this latter can be supplied to the grid by inverting the system operation. The paper shows how to achieve this result by implementing a dedicated control action based on a multi-step procedure. Numerical investigations are carried out on a 19-level CHB converter implemented in the PLECS environment to validate the feasibility and effectiveness of the proposed control technique.

Keywords: cascaded H-bridge; PV generators; battery charger; inverter operation mode

check for updates

Citation: Coppola, M.; Guerriero, P.; Dannier, A.; Daliento, S.; Del Pizzo, A. Inverter Operation Mode of a PhotoVoltaic Cascaded H-Bridge Battery Charger. *Energies* **2023**, *16*, 4972. https://doi.org/10.3390/en16134972

Academic Editor: Carlo Renno

Received: 17 May 2023
Revised: 21 June 2023
Accepted: 24 June 2023
Published: 27 June 2023

1. Introduction

The opportunity of using a multilevel architecture based on the Cascaded H-Bridge (CHB) configuration to charge a battery energy storage system (BESS) was exploited by the authors in previous work [1]. The proposed system comprises photovoltaic generators (PVGs) which represent the primary source to perform its main task of charging the batteries. Nevertheless, the PVGs cannot guarantee short and predetermined charging time as well as the proper power level (i.e., the charging current requested by the battery control), because the PV power is inherently intermittent. Therefore, the CHB is connected to the main grid, and it operates as an active rectifier to provide the difference in power needed for battery charging. One of the advantages of this configuration relies on the possibility of splitting the storage system into smaller units each of which is connected to the separate dc-links of the CHB circuit, leading to a distributed storage system [2–8].

In [2] the CHB is used as a multilevel inverter to directly connect the BESS to the medium voltage (MV) grid. The proposed control approach ensures SOC balancing charge/discharge control as well as fault detection with a reduced number of voltage sensors.

For the same purpose of linking the BESS in a split manner to the MV grid, in [3] the BESS are integrated into a three-phase modular multilevel converter (MMC) with a SOC balancing control. In [4] a method to handle an unbalanced power distribution among the HBs of hybrid BESS in a single-phase CHB/MMC inverter is proposed.

In [5] a review of power inverter topologies for utility BESS is performed. It highlights the advantage of shortening the battery strings when used in multilevel inverters such as the CHB configuration while also obtaining proper SOC balancing.

In [6] the authors proposed a PV module-level single-phase CHB inverter with an integrated BESS to smooth the PV fluctuations and to provide both an energy buffer and

coordination of power supply and demand to obtain a flat profile of the output power, also in case of PV generators mismatch conditions, by ensuring balanced dc-link voltage at the price of SOCs unbalancing. The authors of [7] are the same as [4], so the same issue of unbalanced power distribution among the HBs of hybrid BESS in a single-phase CHB/MMC inverter is considered by taking into account the effect of the capacitor voltage ripple of each sub-module in the multilevel configuration. In [8] a PV module-level three-phase CHB inverter with an integrated BESS is proposed with the same goal of [6] or rather the smoothing of PV intermittency and the compensation of PV unbalance.

In the above papers, the split arrangement of BESS allows the shortening of each battery pack (i.e., a reduced number of battery cells connected in series), thus alleviating the problems due to overcharging and overheating of the storage device, while also mitigating the risk of a shutdown of the battery caused by the failure of a single cell in the string [3]. In addition, the feature of modularity as well as the possibility of providing a redundancy, which is typical of a multilevel circuit configuration, are transferred to the batteries so leading to a more flexible storage system where both the control and the maintenance can be performed separately on each battery unit. Further advantages are the ability to perform distributed maximum power point tracking (DMPPT) and to suitably manage the charging current of the battery units to keep their SOCs balanced. On the other hand, one of the main drawbacks is the possible presence of a power imbalance among the HBs in the cascade, which can drive the more powerful HBs in the overmodulation region [9–11] up to the maximum allowed power for each HB corresponding to the square-wave operation. This issue was addressed in a previous authors' work [1] by implementing a dedicated modulation technique along with a modulation index control allowing it to reach the overmodulation region without a detrimental effect on the system performance. The trouble is obviously present also when the CHB is operated as an active rectifier, as in our proposal, where the BESS represents the load, and the main grid plays the role of guaranteeing short and predetermined charging time as well as the proper power level to charge the batteries, which cannot be ensured by the PVGs due to their inherent intermittent nature. In addition, when a mismatch condition among the PVGs occurs, each HB must handle different power provided by the grid, leading to a power imbalance in the cascade with the consequences previously highlighted.

In this paper, we address a different problem that can occur in the proposed battery charger when the battery SOC overcomes a predefined upper limit beyond which the charging process could be interrupted. In such a case, the PV power production can no longer be transferred to the storage, thus, to avoid an undesirable complete curtailment of the available PV power, the system should be able to invert its operation with the aim of providing the produced PV power to the grid. It means that the system must now work as a grid-connected double-stage PV CHB inverter [12–14].

The main purpose of this paper is to address this issue by implementing a dedicated control action that allows the CHB to switch from the rectifier to the inverter operation mode so that the available PV power can be transferred to the grid. This result can be obtained by a multi-step procedure, which will be detailed in the following.

The paper is organized as follows: Section 2 shows the circuit configuration, while Section 3 shows its main operation. The system control along with the multi-step procedure to invert the operation is discussed in Section 4. Section 5 highlights the obtained numerical results for the case study; finally, conclusions are drawn in Section 6.

2. System Description

The system configuration is shown in Figure 1. It consists of N series connected cells, each of which is composed by the H-Bridge in the cascade, a unidirectional step-up chopper performing the DMPPT, and a bidirectional dc-dc converter devoted to the charge/discharge process of the battery.

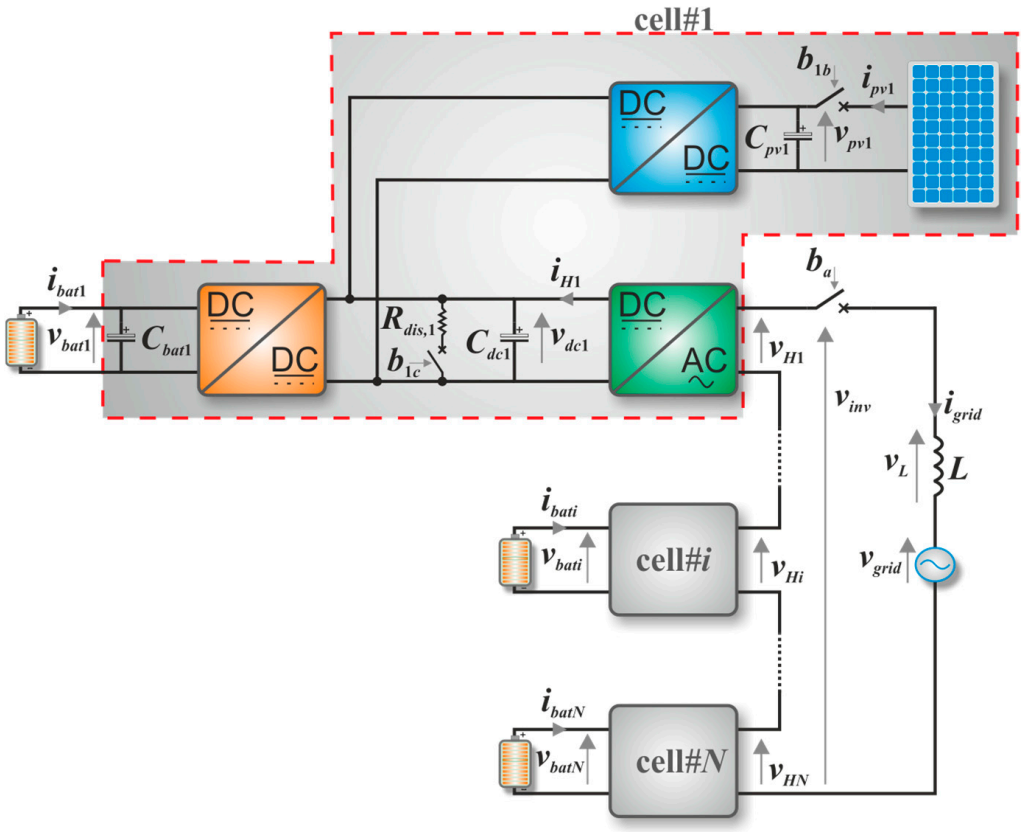

Figure 1. Schematic view of a generic $2N + 1$ level PV CHB battery charger.

The power circuits are detailed in Figure 2. The H-Bridge (Figure 2a) consists of four switches) and a dc-link capacitor C_{dci} suitably chosen to obtain a desired reduced voltage ripple at the rated power level. The unidirectional boost dc-dc converter (Figure 2b) represents the front-end of the individual PVG of each cell. The choice of a boost topology is made to meet the higher voltage level of the dc-link so also ensuring an extended MPP tracking range thus guaranteeing the operation at the MPP also in case of low irradiation level. The presence of the input capacitor C_{pvi} is useful to decouple the high-frequency current ripple, due to the dc-dc converter, from the PVG, while the inductor L_{pvi} is sized by considering the constraint to assure the continuous conduction mode (CCM) operation, which is mandatory for a correct operation of the PVG.

Finally, the bidirectional dc-dc converter (Figure 2c) is responsible for the charging/discharging process of the battery. It consists of a conventional half-bridge (S_{iHbat}, S_{iLbat}), an inductor L_{bati} and a capacitive filter C_{bati} placed on the battery port side. This architecture enables a bidirectional power flow through the reversal of the current direction. In principle, it should only perform the battery charging but the possibility of reversing the power flow can be useful in the case of fulfilling ancillary tasks.

The system also presents three breakers (see Figure 1): b_a, b_{ib} are normally closed and they can, respectively, disconnect the grid and the PV panel when needed, the third one b_{ic} is normally open, while it can be closed to discharge the dc-link capacitor during the procedure to switch from the rectifier to the inverter operation mode, as detailed in the following.

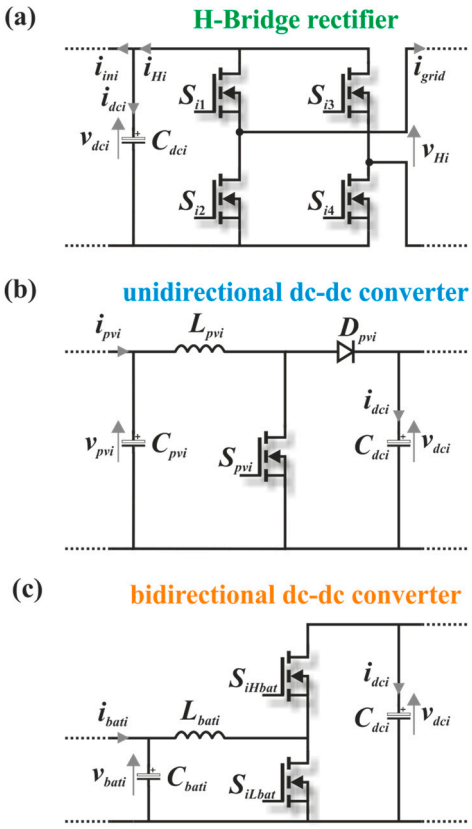

Figure 2. Circuits of the *i*-th cell in the cascade. (**a**) H-Bridge rectifier (**b**) unidirectional dc-dc converter (**c**) bidirectional dc-dc converter.

3. System Operation

Normally the system operates as a battery charger, where it is considered the battery power request (i.e., the charging current) is greater than that provided by the PV panel, thus the grid must supply the remaining power thanks to the CHB working as an active rectifier. In such a case, the system operation can be described as already discussed in [1] and here reported for the sake of clarity. By referring to Figures 1 and 2, the multilevel ac input voltage of the CHB rectifier is $v_{CHB.}$

$$v_{CHB} = \sum_{i=1}^{N} v_{Hi} \tag{1}$$

where the cell input voltage v_{Hi} can be defined as

$$v_{Hi} = (S_{i1} - S_{i3})v_{dci} = s_i v_{dci} \tag{2}$$

S_{ik} ($i = 1, \ldots, N; k = 1, \ldots, 4$) is the logic state of the switching signal of the *k*-th power semiconductor device in the *i*-th HB as shown in Figure 2a, while s_i is the corresponding continuous switching function.

The dynamic behavior of the system is given by

$$\frac{di_{grid}}{dt} = \frac{v_{CHB} - v_{grid}}{L} = \frac{\sum_{i=1}^{N} s_i v_{dci} - v_{grid}}{L} \tag{3}$$

$$i_{ini} = C_{dci}\frac{dv_{dci}}{dt} - i_{Hi} \quad i = 1, \ldots, N \tag{4}$$

where i_{grid}, v_{grid} are the grid current and voltage, v_{dci} and i_{ini} are the dc-link voltage and the input current of the i-th cell, while i_{Hi} is the output current of i-th HB rectifier

$$i_{Hi} = s_i i_{grid} \quad i = 1, \ldots, N \tag{5}$$

and

$$i_{dci} = C_{dci} \frac{dv_{dci}}{dt} \quad i = 1, \ldots, N \tag{6}$$

is the current of the i-th dc-link capacitor.

The main task of the proposed system is to charge the batteries, while also keeping their SOC balanced. Nevertheless, when the batteries' SOC overcomes a predefined upper limit, the battery unit of each cell must be disconnected from the main circuit and the system must behave as a grid-tie PV CHB inverter to provide the grid with the available PV power, thereby helping to prevent the loss of the produced PV energy due to an undesired, but needed curtailment of PV power if the system is not able to invert its operation. A major part of the system control remains the same as proposed in [1] with some additional tricks that will be detailed in the following section.

4. Control Strategy

The control architecture is shown in Figure 3. It comprises three main sections: one devoted to the control of PV power (Figure 3a) by means of an MPPT algorithm executed for each single PV module; the second section is dedicated to the control of charging/discharging of the storage unit (Figure 3b); the last section represents the CHB rectifier control and modulator stage (Figure 3c). The details of the proposed control strategy for rectifier operation are reported in [1], and here briefly reported for the sake of clarity and completeness.

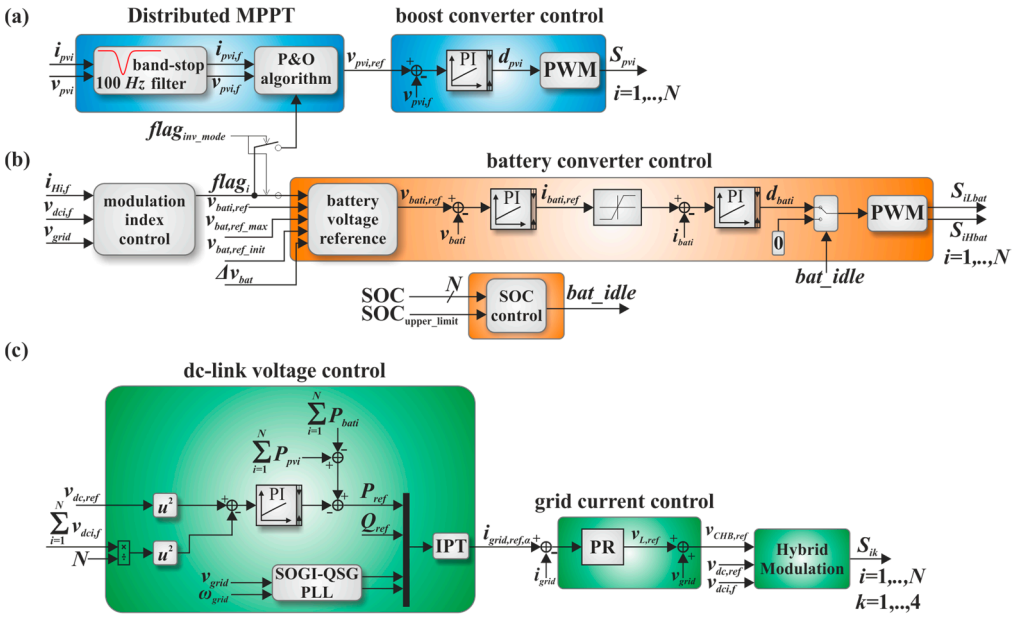

Figure 3. Block diagram of the proposed control technique: (**a**) DMPPT and unidirectional boost dc-dc converter control; (**b**) battery converter control along with modulation index control; (**c**) CHB rectifier control and modulator stage.

4.1. PV Converter Control

The MPPT performed on the single PV module included in each cell is based on a conventional Perturb&Observe algorithm using an MPPT time step equal to 50 ms with a fixed voltage reference step of 0.3 V. As can be inferred from Figure 3a, the measured input quantities (i.e., PV voltage and current) are properly filtered and then processed by the

MPPT block to obtain the desired PV voltage reference. The voltage error goes to the input of a PI regulator whose output is the duty-cycle of the PV converter (see Figure 2b).

4.2. Battery Converter Control

By strictly considering the battery converter control scheme included in the orange area of Figure 3b, the battery voltage error is processed by a PI regulator to carry out the desired battery current reference which passes through a saturation block to fix the maximum permitted current. Then, the obtained current error is the input of the second PI outgoing the converter duty-cycle. Now, it must be highlighted that the battery voltage reference is derived from the battery voltage reference block (Figure 3b) where the first input is represented by a flag signal provided by the modulation index control whose action is detailed in the following sub-section.

4.3. Modulation Index Control

The normal operation of the proposed system is like a battery charger so that the CHB operates in rectifier mode. In fact, as anticipated in the previous section, the operating principle is since the power request for battery charging is always greater than the power produced by the PV panel. Therefore, the grid must provide the difference power which means that the CHB is operated in rectifier mode.

In uniform conditions, each PV panel is under the same irradiance level, and similarly, each battery explores the same initial SOC. As a consequence, each battery requires the same power meaning the difference power provided by the grid is evenly distributed among the N HBs hence handling the same power (i.e., the total grid power divided by N). In such a case, the CHB is balanced, and each HB works in the linear modulation region.

On the contrary, a relevant issue that affects the CHB architecture is related to the power imbalance among the HBs. In fact, in this condition, the more powerful HBs can reach the overmodulation region due to the higher power content to be managed, which is directly related to the amplitude of the corresponding voltage modulation index [1,10]:

$$m_i = \frac{v_{grid,max}}{\frac{1}{i_{Hi,f}} \sum_{j=1}^{N} i_{Hj,f} v_{dcj,f}} \quad i = 1, \ldots, N \tag{7}$$

where $v_{grid,max}$ is the peak value of the grid voltage (i.e., $\sqrt{2}\cdot 230$ V). The dc-link voltage $v_{dci,f}$ and the HB current $i_{Hi,f}$ are obtained from a 100 Hz band-stop filter to cancel the second harmonic component arising from the single-phase connection to the grid. The modulation index control block (see Figure 3b) verifies if the modulation index m_i (calculated by using (7)) is greater than a predefined upper limit (or rather if the HB is in overmodulation), then, if so, a flag signal ($flag_i$ in Figure 3b) becomes high (i.e., 1 logic level). Then, the battery voltage reference, $v_{bati,ref}$, is decreased by a fixed quantity Δv_{bat} with the aim of reducing the battery current reference (i.e., reducing the power request from the corresponding cell) to guarantee a stable system operation. The modulation index calculation and control is performed every 50 ms (i.e., the same execution time as the MPPT control).

The possibility of the modulation index to overcome the unity with no harmful impact on the harmonic content of the converter is due to the hybrid modulation technique proposed by the authors in [1,10,15].

4.4. Hybrid Modulation

The used hybrid modulation involves a sorting algorithm to obtain a sorted vector of the dc-link errors (i.e., $v_{dci,f} - v_{dci,ref}$) in ascending order. The main purpose is to charge/discharge each dc-link to reach the desired voltage reference by also achieving a proper synthesis of the CHB voltage reference. To do this, each HB can be in four different states: +1 state (corresponding to a HB voltage equal to $+v_{dci}$); −1 state (corresponding to a HB voltage equal to $-v_{dci}$); 0 state (corresponding to a HB voltage equal to 0); PWM state

(corresponding to a HB voltage equal to a PWM voltage). The choice of each HB state is performed with a sorting time of 0.25 ms.

4.5. CHB Control

Finally, the main control loop of the CHB rectifier is shown in Figure 3c. It is the cascade of two control loops: the first one is dedicated to the control of the dc-link voltage-squared by means of a proportional-integral (PI) regulator whose output represents the active power compensated by the difference between the PV and battery power, thus resulting in the active power reference, P_{ref}. The subsequent block is based on the instantaneous power theory (IPT) [16], where the voltages and currents are expressed in the stationary reference frame, or rather the positive and negative sequence of the grid current are functions of the desired instantaneous active (P_{ref}) and reactive power (Q_{ref}). The quantities in the $\alpha\beta$ coordinates result from a second-order generalized integrator (SOGI) [17,18] to obtain a quadrature signal generation (QSG). Obviously, in a single-phase system, only the α component is considered, $i_{grid,ref,\alpha}$. The grid current error is the input of a proportional-resonant (PR) regulator, which outputs the line inductor voltage reference $v_{L,ref}$. This latter is then summed to the measured grid voltage to produce the CHB voltage reference, $v_{CHB,ref}$.

4.6. Multi-Step Procedure: Switch from Rectifier to Inverter Operation Mode

The SOC control verifies if the SOCs overcome a preset upper limit (i.e., $\text{SOC}_{\text{upper\_limit}}$ in Figure 3b). When this event occurs, the battery idle signal (i.e., *bat_idle* in Figure 3b) goes high, and the duty cycle of the battery converter is set to zero thus disconnecting the battery from the main circuit. In this case, the PV power can no longer be transferred to the battery, thus it is necessary to invert the CHB operation if you want to provide this energy to the grid avoiding an undesired curtailment of the PV power production. As already stated in the introduction, our main purpose is to address this issue by implementing a dedicated control strategy, which is based on a multi-step procedure. Figure 4 shows the main execution times of this latter along with the main tasks performed at each time instant. The provided steps are the following:

- Battery idle goes high (i.e., 1 logic level) and we can consider this event as the start time of the procedure (t_1). At this time the breakers b_a, b_{ib} (see Figure 1) are open so physically disconnecting the main grid and the PV panels from the circuit, while the HBs and the PV converters are switched off by setting to the zero-logic level the correspondent command signals (S_{pvi}, S_{ik}) as well as the battery converter duty cycle (d_{bati}) to disconnect the battery. On the other hand, the breakers b_{ic} are closed to allow the discharge of the dc-link capacitors. Additionally, all the control blocks are frozen.
- At the time $t_2 = t_1 + \Delta t_{grid}$, the breakers b_{ic} are open and the breaker b_a is closed, thus the grid is reconnected while each HB represents a diode bridge (formed by the body diodes of the power semiconductor devices of the bridge itself) by considering that at the time t_1 all the switching signals S_{ik} are set to zero-logic level. In such a case, the CHB behaves as a passive rectifier and allows to charge each dc-link capacitor at the same voltage level equal to $v_{grid,\max}/N$.
- At the time $t_3 = t_2 + \Delta t_{control}$, the breakers b_{ib} are closed to reconnect the PV panels. Simultaneously, all the controls are reactivated and the HBs and the PV converters are switched on. Moreover, the inverter mode flag (see Figure 3) goes high, thus transferring the management of the modulation index control to the MPPT algorithm. This latter because now the power handled by each HB is the PV power.

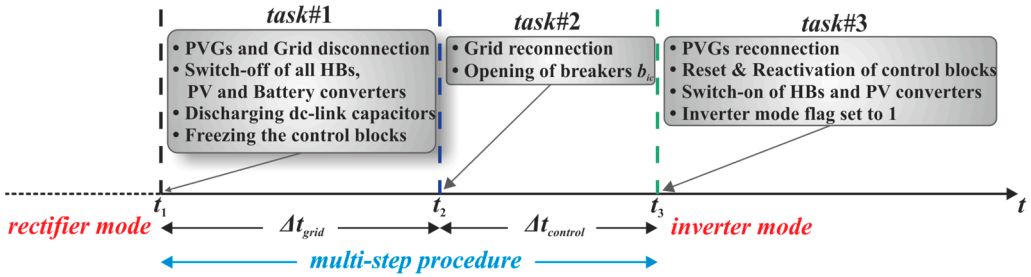

Figure 4. Multi-step procedure: execution times and performed tasks.

4.7. Inverter Mode

The operation as an inverter starts after the multi-step procedure described above. In practice, the system control is still the same with the difference that the battery is disconnected, the reason for which the modulation index control flag is now routed to the MPPT control block thanks to the $flag_{inv\_mode}$ signal (see Figure 3a). In fact, in such a case, the possible power imbalance among the HBs arises from a different power provided by the PV generators due to different irradiance levels. Consequently, if the modulation index m_i becomes greater than a predefined upper limit the PV voltage reference, $v_{pvi,ref}$, is increased by a fixed quantity Δv_{pvi} with the aim of reducing the PV current/power so ensuring a stable circuit operation. The control section remains practically the same by simply excluding the battery converter control as shown in Figure 5. The other main difference is that now the dc-link voltage error for the hybrid modulation block is calculated as $v_{dci,ref} - v_{dci,f}$.

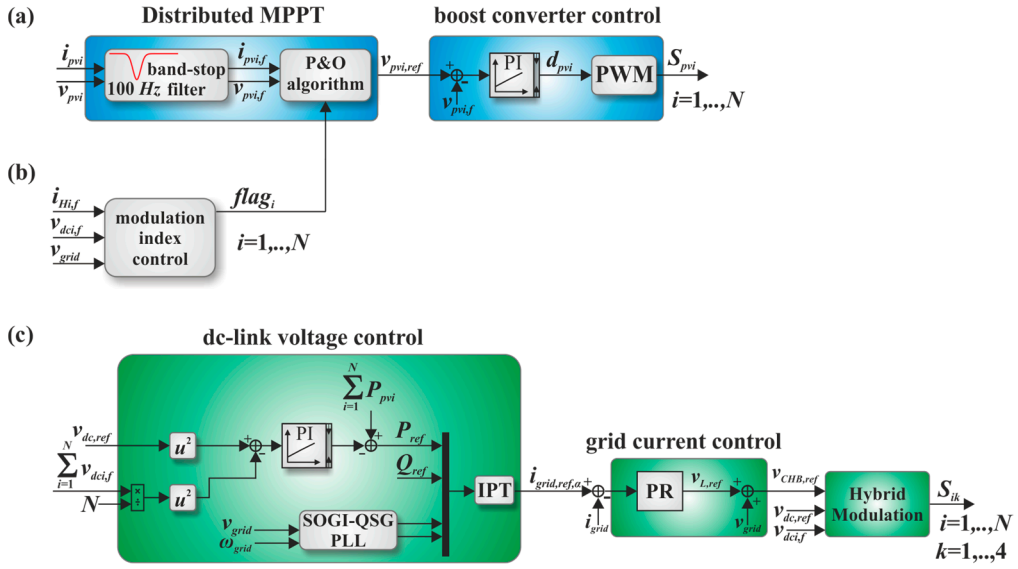

Figure 5. Control section during inverter operation mode: (**a**) DMPPT and unidirectional boost dc-dc converter control; (**b**) modulation index control; (**c**) CHB inverter control and modulator stage.

5. System Performance

The proposed system is made up of N = 9 cells, thus forming a 19-level CHB. The system performance is simulated in the PLECS environment by implementing an average model of the power converters to reduce the computational effort without affecting the obtained results. Moreover, only one of the nine cells must be explicitly drawn thanks to the possibility offered by PLECS to obtain a vectorized simulation model where the single cell is internally multiplexed N times.

The used physical model of the PV module is a generalization of the well-known five-parameter single diode model. At standard test condition (STC) the operating point is determined as P_{MPP} = 331.55 W, V_{MPP} = 37.6 V and I_{MPP} = 8.82 A being the power, voltage

and current at MPP, respectively. The PV model is implemented in a C-script block where it is also possible to properly allocate the memory in order to handle the vectorized model.

The simplified model of the battery provides for a logarithmic dependence of the open circuit voltage (V_{oci}) from the SOC

$$\begin{aligned} V_{oci} &= E_0 + \frac{RT}{F}\log\left(\frac{SOC_i}{1-SOC_i}\right) \\ SOC_i(t) &= SOC_i(t_0) - \frac{\int_{t_0}^{t} i_{bati}d\tau}{Q_0} \end{aligned} \tag{8}$$

where E_0 is the standard potential of the battery, R is the ideal gas constant, T is the absolute temperature and F is the Faraday constant, and Q_0 is the battery maximum charge. The battery equivalent circuit comprises an ideal voltage source V_{oci}, in series with a constant internal resistance R_{int}. Generally, both these latter parameters depend on the SOC and the temperature, but only the dependency of the V_{oci} on the SOC has been considered in Equation (8) to simplify the model. The used battery features a capacity of 20 Ah, a rated voltage of 38.4 V, and an internal resistance R_{int} = 7.5 mΩ.

The values of the input quantities of the battery voltage reference block in Figure 3b are: v_{bati,ref_max} = 44.1 V (i.e., the maximum permissible voltage); v_{bati,ref_init} = 41.25 V (i.e., the initial battery voltage); Δv_{bat} = 0.285 V (i.e., the battery voltage reference step). As per the PV model, the battery model (Equation (8)) is implemented in a C-script block whose output V_{oc} represents the input of the ideal controlled voltage source in series with the internal resistance in the circuital model. Moreover, by referring to Figure 3, the modulation index control, the battery voltage reference, the IPT and the hybrid modulation blocks are implemented in the C-script control block of the PLECS library. The three breakers (see Figure 1): b_a, b_{ib}, and b_{ic} are implemented with multi-position switches properly controlled by the battery idle signal to respect the timing defined by the multi-step procedure described in Section 4.6.

The values of the used circuit and control parameters are listed in Table 1. The passive components were designed by considering [19,20]. Specifically, the line inductance L and the dc-link capacitance C_{dci} were chosen to obtain a desired current and voltage ripple at the nominal power conditions not greater than 2% and 10%, respectively [19]. The PV capacitance C_{pvi} was chosen to decouple the high-frequency current ripple due to the boost converter from the PVG [20], while the value of the inductances L_{pvi} and L_{bati} were sized to ensure the CCM operation of both dc-dc converters.

Table 1. Used circuit and control parameters.

Circuit Parameter	Value	Control Section	Control Parameter	Value
$v_{grid,max}$	~325 V	PV converter (PI)	k_p	1×10^{-5}
f_{grid}	50 Hz		k_i	2
$v_{dc,ref}$	48 V	Battery converter (outer loop PI)	k_p	2
L	10 mH		k_i	1×10^{-6}
R	0.8 Ω	Battery converter (inner loop PI)	k_p	0.1
C_{dci}	6 mF		k_i	10
$R_{dis,i}$	1 Ω	CHB converter (PI)	k_p	1
C_{pvi}	50 µF		k_i	100
C_{bati}	100 µF	CHB converter (PR)	k_p	35
L_{pvi}	2 mH		k_r	1×10^2
L_{bati}	2 mH	SOGI	k	1.414

The parameters of the PI regulators were chosen to obtain a desired settling time and steady-state error [21] by also considering that the controllers of the three power conversion stages can be considered independent of each other thanks to the decoupling action of the dc-link capacitor whose voltage, as a first approximation, can be considered constant.

The resonant controller was useful to introduce an infinite gain at a selected resonant frequency (i.e., the grid frequency in our case) for eliminating steady-state error at that frequency. Practically, it acts similarly to an integrator whose infinite dc gain ensures the steady-state error goes to zero. When it is associated with a proportional term, the ideal PR regulator is obtained [22]. The proportional gain can be chosen as per the PI controller, while the integral constant, which determines the bandwidth centered at the resonance frequency, can be chosen high enough to reach the desired behavior. The value of k_r was determined by simulations in order to eliminate the steady error at the grid frequency.

The simulation set-up was properly conceived to test the ability of the proposed system to switch from the rectifier operation, as a battery charger, to the inverter mode, as a grid-connected PV-CHB inverter. The considered conditions are the following:

- all the PV modules are subjected to the same irradiance level equal to 1000 W/m^2 (Standard Test Condition, STC) or rather static uniform conditions.
- all the batteries exploit the same starting conditions corresponding to a SOC level equal to 50%, while the SOC_{upper_limit} is set to 50.02% (i.e., an increase of only 0.02% with respect to the initial value to allow a reasonable simulation time).

The main goal of the numerical investigation is to verify that the system is able to reach, in a suitable time, a steady-state behavior after the inversion of the operating condition. In fact, initially, the CHB behaves as an active rectifier to fulfill the main system function of a battery charger. It reaches the steady state, then, when the SOC_{upper_limit} is exceeded, the multi-step procedure, described in Section 4, can start so leading to the switch from the rectifier to the inverter operation mode. Figure 6 shows the dc-link time behavior.

In particular, Figure 6b shows the zoom view to identify the main time instants (t_1, t_2, t_3) of the multi-step procedure to switch to the inverter operation mode. In fact, in Figure 6a the system steady-state behavior of the dc-link voltages before t_1, when the CHB behaves as an active rectifier can be seen. At the instant t_1 the SOC overcomes the predefined upper limit (see Figure 7), the battery idle flag goes high starting the multi-step procedure to disconnect the batteries and to invert system operation.

(**a**)

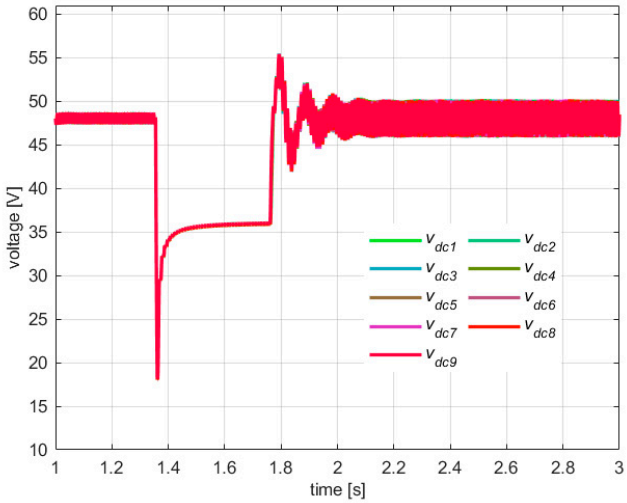

Figure 6. *Cont.*

(**b**)

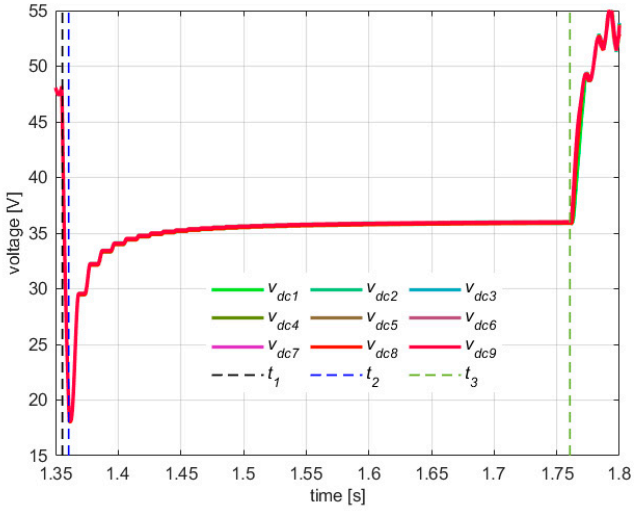

Figure 6. Time behavior of dc-link voltages: (**a**) full view starting from the steady-state reached during rectifier operation mode; (**b**) zoom view to identify the main time instants (t_1, t_2, t_3) of the multi-step procedure to switch to the inverter operation mode.

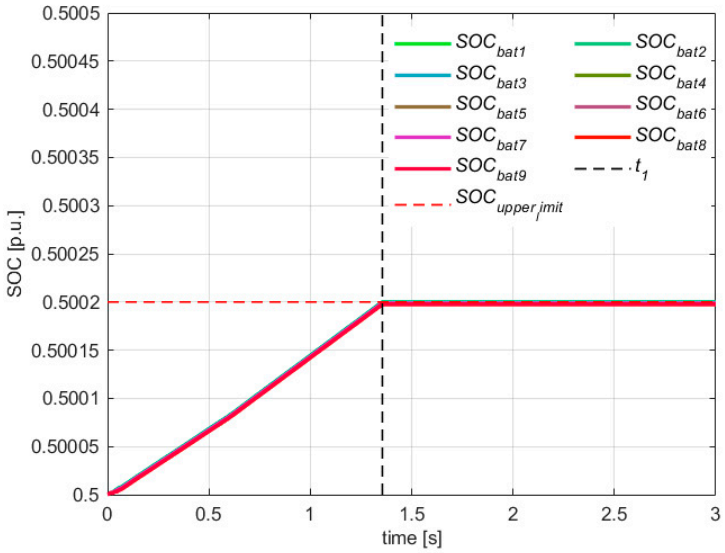

Figure 7. Time behavior of the SOCs.

As explained above, at time t_1 the breakers b_a, b_{ib} are open to disconnect the grid and the PV panels, while all the switching signals (S_{pvi}, S_{ik}, S_{iLbat}, S_{iHbat}) are set to the low logic level to switch off all the power devices. In addition, all the control blocks are frozen. Instead, the breakers b_{ic} are closed to discharge the dc-link capacitors through the discharging resistors $R_{dis,i}$, which is properly chosen to ensure the discharge happens in a short time interval Δt_{grid} = 5 ms. The latter is equal to t_2-t_1 as can be inferred from Figure 6b, where the dc-link voltages starting from the steady-state value of 48 V fall down to a value lower than 20 V.

At the time $t_2 = t_1 + \Delta t_{grid}$, the breaker b_a is closed, thus reconnecting the system to the utility network, while the breakers b_{ic} are open. In such a situation, the dc-link capacitors can be charged by the grid through the CHB which behaves as a passive rectifier. In fact, each HB in the cascade is now a diode bridge formed by the body diodes of the power semiconductor devices. After the time interval $\Delta t_{control}$ = 400 ms, the dc-link voltages reach the same level equal to $v_{grid,\max}/N$ because the grid power is evenly distributed among the cells. In our case, N = 9 and $v_{grid,\max} \cong$ 325 V, thus leading to a voltage level of about 36 V at each dc-link, as can be seen in Figure 6.

Once reached this condition at time $t_3 = t_2 + \Delta t_{control}$, the breakers b_{ib} are closed to reconnect the PV panels. Simultaneously, all the control blocks are first reset and then reactivated and the HBs and the PV converters are switched on. Moreover, the inverter mode flag (see Figure 3) goes high, thus transferring the management of the modulation index control to the MPPT algorithm.

As shown in Figure 6, after a short transient time a steady-state behavior is reached where the dc-link voltages follow the desired reference of 48 V but with a wider oscillation w.r.t. the previous operation mode due to a higher power to be handled by each HB. Figure 8 reports the power behavior. In the first part, during the batteries' charging process, the power is mainly provided by the PV panels, while only the residual part is provided by the grid to fulfill the batteries' request. After the time instant t_3, all the PV power is transferred to the grid to avoid an undesired curtailment of the available PV power.

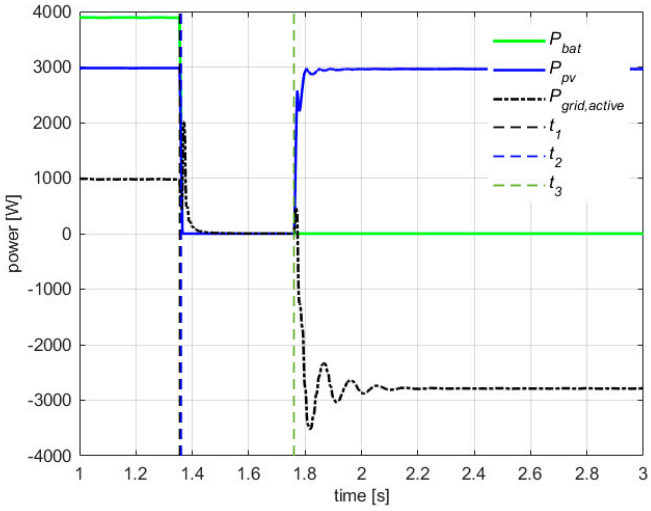

Figure 8. Power behavior: PV power (blue line), battery power (green line), grid active power (dot-dashed black line).

Finally, the grid behavior is shown in Figure 9 to further highlight the effectiveness of the proposed control strategy.

(**a**)

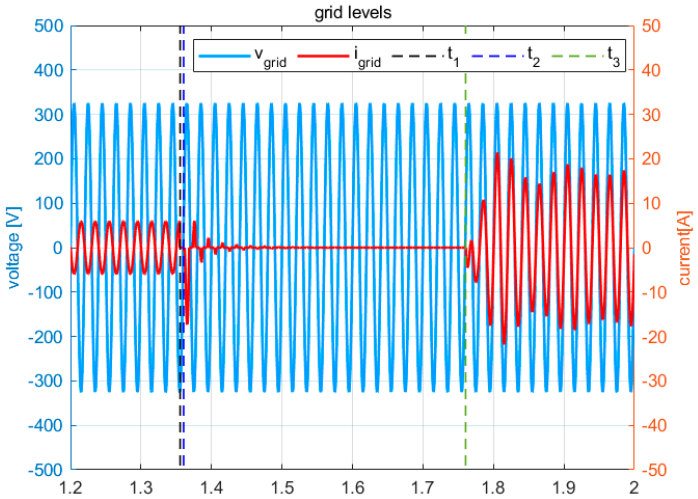

Figure 9. *Cont.*

(**b**)

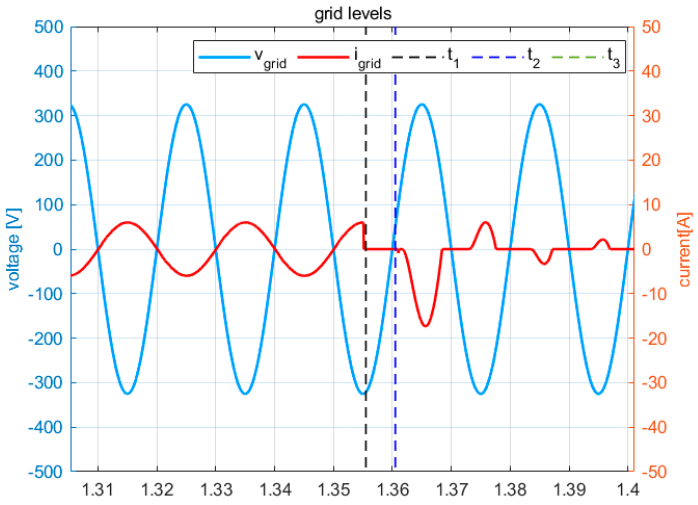

(**c**)

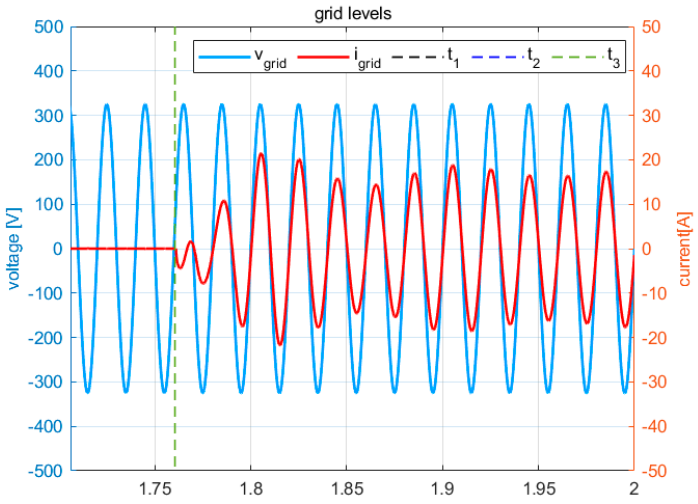

Figure 9. Time behavior of grid voltage and current: (**a**) zoom view starting from the steady-state reached during rectifier operation mode until the inverter operation mode; (**b**) zoom view to identify the first time instants t_1 and t_2 of the multi-step procedure; (**c**) zoom view to identify the time instant t_3 which coincides with the end of the multi-step procedure and the beginning of the inverter operation mode.

Before the time instant t_1, the system is in the rectifier operation mode. The grid current is in phase opposition w.r.t. the grid voltage by considering the current sign in Figure 1. At time t_1 the grid current goes to zero (see Figure 9b) until t_2 when the grid is reconnected to charge the dc-link capacitors. Then, at time t_3 (see Figure 9c) or rather at the end of the multi-step procedure, the inverter operation mode starts. As can be inferred from Figure 9c, the control is able to follow the desired reference in a very short time, so that the PVGs provide their power to the grid with a practically unit power factor and a grid current THD of about 0.3%, well below the maximum upper limit of 5% required by the standard rules for a grid-connected application.

6. Conclusions

This paper is mainly focused on the possibility of rapidly inverting the operation of the CHB battery charger when the SOCs overcome a preset upper limit. This requirement is due to the presence of the PVGs, which represent the primary source to charge the batteries also if the grid support is mandatory to reach the desired charging power. When this task can no longer be fulfilled because the batteries have reached the chosen SOC level, the available PV power would be lost. To avoid the undesired curtailment of PV power,

the proposed control strategy, consisting of a multi-step procedure, can switch the CHB operation from the rectifier to the inverter mode, while also ensuring in a very short time interval to achieve the desired behavior of the double-stage PV CHB inverter. It is worth noting that the use of the CHB circuit in rectifier operation mode to support the PVGs in charging a split BESS is not yet so widespread. Consequently, we have first addressed the overmodulation issue which is related to the power imbalance in the multilevel architecture independently from the operation mode (i.e., inverter or rectifier). A possible solution is a hybrid modulation strategy along with a suited modulation index control which must act on the battery voltage reference when the system is operated as a battery charger. The control action ensures an extended operating range of the CHB circuit also in case of power mismatch among the HBs in the cascade. Nevertheless, in the proposed battery charger the possibility of stopping the batteries' charging process must be considered. In such a situation, the produced PV power can no longer be provided to the storage system, thus the only possibility to avoid its curtailment is to invert the CHB operation so that the PV generation can be directed to the utility network. Therefore, the main purpose of this paper is to address this issue by implementing a dedicated multi-step procedure allowing the CHB to switch from the rectifier to the inverter operation mode. During the inverter operation mode, the control action remains practically the same by excluding the battery converter control, the reason why the modulation index control must be routed to the MPPT control to properly act on the PV voltage reference.

The proposed multilevel converter architecture represents the possibility of properly charging a split accumulation system by primarily using a renewable energy source whose production can still be used also when the battery charging is stopped thanks to the inversion of the CHB operating mode. A complete set of simulated performances proved the effectiveness of the proposed circuit and controller design.

Author Contributions: Conceptualization, M.C. and P.G.; methodology, M.C. and P.G.; software, M.C., P.G. and A.D.; validation, M.C., P.G., A.D., S.D. and A.D.P.; formal analysis, M.C., P.G. and A.D.; investigation, M.C., P.G. and A.D.; resources, S.D. and A.D.P.; data curation, M.C. and P.G.; writing—original draft preparation, M.C.; writing—review and editing, A.D.P., S.D. and A.D.; visualization, M.C., P.G. and A.D.; supervision, A.D.P. and S.D. All authors have read and agreed to the published version of the manuscript.

Funding: This research received no external funding.

Data Availability Statement: The data are not publicly available due to privacy restrictions.

Conflicts of Interest: The authors declare no conflict of interest.

References

1. Dannier, A.; Guerriero, P.; Coppola, M.; Daliento, S.; Pizzo, A.D. A Battery Charger based on Cascaded H-Bridge Rectifier with integrated PV Generators. In Proceedings of the 2022 International Symposium on Power Electronics, Electrical Drives, Automation and Motion (SPEEDAM), Sorrento, Italy, 22–24 June 2022; pp. 324–329. [CrossRef]
2. Gorla Yadav, N.B.; Farivar, G.G.; Liang, G.; Beniwal, N.; Ezequiel, R.R.; Pou, J. Operation of Cascaded H-bridge-Based Split-Battery Energy Storage System with Reduced Sensors. In Proceedings of the 2021 IEEE 12th Energy Conversion Congress & Exposition—Asia (ECCE-Asia), Singapore, 24–27 May 2021; pp. 1572–1577.
3. Vasiladiotis, M.; Rufer, A. Analysis and Control of Modular Multilevel Converters with Integrated Battery Energy Storage. *IEEE Trans. Power Electron.* **2015**, *30*, 163–175. [CrossRef]
4. Liang, G.; Farivar, G.G.; Ceballos, S.; Tafti, H.D.; Pou, J.; Townsend, C.D.; Konstantinou, G. Unbalanced Active Power Distribution of Cascaded Multilevel Converter-Based Battery Energy Storage Systems. *IEEE Trans. Ind. Electron.* **2022**, *69*, 13022–13032. [CrossRef]
5. Wang, G.; Konstantinou, G.; Townsend, C.D.; Pou, J.; Vazquez, S.; Demetriades, G.D.; Agelidis, V.G. A Review of Power Electronics for Grid Connection of Utility-Scale Battery Energy Storage Systems. *IEEE Trans. Sustain. Energy* **2016**, *7*, 1778–1790. [CrossRef]
6. Sirico, C.; Teodorescu, R.; Séra, D.; Coppola, M.; Guerriero, P.; Iannuzzi, D.; Dannier, A. PV Module-Level CHB Inverter with Integrated Battery Energy Storage System. *Energies* **2019**, *12*, 4601. [CrossRef]
7. Liang, G.; Tafti, H.D.; Farivar, G.G.; Pou, J.; Townsend, C.D.; Konstantinou, G.; Ceballos, S. Effect of Capacitor Voltage Ripples on Submodule Active Power Control Limits of Cascaded Multilevel Converters. *IEEE Trans. Ind. Electron.* **2022**, *69*, 5952–5961. [CrossRef]

8. Nayak, S.; Das, A.; Torres-Olguin, R.E.; D'Arco, S.; Guidi, G. Battery Energy Support to Cascaded H-Bridge Converter-Fed Large-Scale PV System During Unbalanced Power Generation. *IEEE Trans. Ind. Appl.* **2022**, *58*, 7479–7489. [CrossRef]
9. Miranbeigi, M.; Iman-Eini, H. Hybrid Modulation Technique for Grid-Connected Cascaded Photovoltaic Systems. *IEEE Trans. Ind. Electron.* **2016**, *63*, 7843–7853. [CrossRef]
10. Coppola, M.; Guerriero, P.; Iannuzzi, D.; Daliento, S.; Del Pizzo, A. Extended operating range of PV module-level CHB inverter. *Int. J. Electr. Power Energy Syst.* **2020**, *119*, 105892. [CrossRef]
11. Zhao, T.; Chen, D. A Power Adaptive Control Strategy for Further Extending the Operation Range of Single-Phase Cascaded H-Bridge Multilevel PV Inverter. *IEEE Trans. Ind. Electron.* **2022**, *69*, 1509–1520. [CrossRef]
12. Wang, M.; Zhang, X.; Zhao, T.; Zhuang, F.; Wang, F.; Qian, N.; Yang, S. Module Power Balance Control Strategy for Three-Phase Cascaded H-Bridge PV Inverter under Unbalanced Grid Voltage Condition. *IEEE J. Emerg. Sel. Top. Power Electron.* **2021**, *9*, 5657–5671. [CrossRef]
13. Yang, S.; Zhang, X.; Mao, W.; Hu, Y.; Wang, M.; Wang, F.; Cao, R. Quantitative Comparison and Analysis of Different Power Routing Methods for Single-Phase Cascaded H-Bridge Photovoltaic Grid-Connected Inverter. *IEEE Trans. Power Electron.* **2021**, *36*, 4134–4152. [CrossRef]
14. Ko, Y.; Andresen, M.; Wang, K.; Liserre, M.G. Modulation for Cascaded Multilevel Converters in PV Applications with High Input Power Imbalance. *IEEE Trans. Power Electron.* **2021**, *36*, 10866–10878. [CrossRef]
15. Iannuzzi, D.; Coppola, M.; Guerriero, P.; Dannier, A.; Pizzo, A.D. Power Scheduling Method for Grid Integration of a PV-BESS CHB Inverter with SOC Balancing Capability. *IEEE Access* **2022**, *10*, 112273–112285. [CrossRef]
16. Akagi, H.; Watanabe, E.H.; Aredes, M. *Instantaneous Power Theory and Applications to Power Conditioning*, 2nd ed.; IEEE Press: Piscataway, NJ, USA, 2017.
17. Blahnik, V.; Kosan, T.; Peroutka, Z.; Talla, J. Control of a Single-Phase Cascaded H-Bridge Active Rectifier Under Unbalanced Load. *IEEE Trans. Power Electron.* **2018**, *33*, 5519–5527. [CrossRef]
18. Ciobotaru, M.; Teodorescu, R.; Blaabjerg, F. A new single-phase PLL structure based on second order generalized integrator. In Proceedings of the 2006 37th IEEE Power Electronics Specialists Conference, Jeju, Republic of Korea, 18–22 June 2006; pp. 1–6.
19. Kjær, S.B. *Design and Control of an Inverter for Photovoltaic Applications*; Institut for Energiteknik, Aalborg Universitet: København, Denmark, 2005.
20. Petrone, G.; Ramos-Paja, C.A.; Spagnuolo, G. *Photovoltaic Sources Modeling*; Wiley-IEEE Press: Piscataway, NJ, USA, 2017; p. 208. ISBN 978-1-118-67903-6.
21. Petrone, G.; Ramos-Paja, C.A.; Spagnuolo, G. *Feedback Systems*; Princeton University Press: Princeton, NJ, USA, 2011.
22. Teodorescu, R.; Blaabjerg, F.; Liserre, M.; Loh, P.C. Proportional-resonant controllers and filters for grid-connected voltage-source converters. *IEE Proc. Electr. Power Appl.* **2006**, *153*, 750–762. [CrossRef]